

EPR Analysis of Spin Susceptibility and Line Width in the Hyperexpanded Fulleride $(\text{CH}_3\text{NH}_2)\text{K}_3\text{C}_{60}$

Alexey Yu. Ganin,[†] Yasuhiro Takabayashi,[‡] Matej Pregelj,[§] Andrej Zorko,[§] Denis Arčon,^{*,§} Matthew J. Rosseinsky,^{*,†} and Kosmas Prassides^{*,‡}

Department of Chemistry, University of Liverpool, Liverpool L69 7ZD, United Kingdom, Department of Chemistry, University of Durham, Durham DH1 3LE, United Kingdom, and Institute Jožef Stefan, Jamova 39, 1000 Ljubljana, Slovenia

Received January 3, 2007. Revised Manuscript Received April 15, 2007

The electron paramagnetic resonance (EPR) technique is used to study the temperature evolution of the electronic and magnetic properties of the hyperexpanded fulleride $(\text{CH}_3\text{NH}_2)\text{K}_3\text{C}_{60}$ in the temperature range 4–294 K. Unambiguous signatures for the development of large internal magnetic fields and a transition to an antiferromagnetic ground state below $T_N = 11$ K are provided by the temperature dependence of the spin susceptibility, the EPR line width, and the position of the EPR line. The EPR results in the paramagnetic regime are indicative of an insulating electronic state, with localized $S = 1/2$ moments on the C_{60}^{3-} ions. The accompanying complex evolution of the spin susceptibility, EPR line width, and *g*-factor anisotropy furthermore reveals that effects of electronic origin (t_{1u} orbital order–disorder transition, crossover from static to dynamic Jahn–Teller distortions) in the vicinity of the structural transformation are important for the understanding of the exchange interactions between the fulleride ions.

Introduction

Current research on metal intercalated fullerenes with stoichiometry A_3C_{60} (A = alkali metal) is driven by the realization that they form an important class of strongly correlated electron systems.^{1–5} Such behavior derives from the unique electronic and crystal structures of these molecular systems and is related to the comparable energy scales of the on-site coulomb repulsion, U , and the width of the half-filled t_{1u} band, W . The superconducting transition temperature, T_c , increases monotonically with increasing interfulleride separation, d (i.e., decreasing bandwidth W), until a critical value is reached when electron correlation effects become dominant and the t_{1u} electrons become localized. The transition to a Mott–Hubbard antiferromagnetic (AF) insulating state occurs when the interfulleride separation increases sufficiently for (U/W) to exceed a critical value of ~ 2.5 and/or the t_{1u} orbital degeneracy is removed through crystal symmetry lowering.^{6,7}

The most successful chemical means of achieving large interfulleride separations has been the solvation of the

intercalated alkali metal ions with a neutral molecule, such as ammonia.⁸ This has allowed the synthesis of a variety of expanded fullerenes and investigation of the electronic properties at volumes beyond those accessible with the bare cations. A prominent success of this strategy has been the synthesis of the antiferromagnetic $(\text{NH}_3)\text{K}_3\text{C}_{60}$ phase ($T_N = 40$ K),^{9–14} which lies exactly at the boundary of the metal–insulator transition and can be transformed into a superconductor by the application of pressure ($T_c = 28$ K).¹⁵ The magnetic exchange interactions in $(\text{NH}_3)\text{K}_3\text{C}_{60}$ sensitively depend on the relative orientation of the near-neighbor C_{60} units.^{12,16–18} The active role played by the C_{60} orientational degrees of freedom in the electronic and magnetic response of $(\text{NH}_3)\text{K}_3\text{C}_{60}$ is reminiscent of the analogous strong coupling between the orbital, charge, spin, and lattice responses in other strongly correlated systems like the CMR manganates. The interfulleride separation can be increased

- * Corresponding author. E-mail: denis.arcon@ijs.si (D.A.); M.J.Rosseinsky@liverpool.ac.uk (M.J.R.); K.Prassides@durham.ac.uk (K.P.).
- † University of Liverpool.
- ‡ University of Durham.
- § Institute Jožef Stefan.
- (1) Gunnarsson, O. *Alkali-Doped Fullerenes*; World Scientific: Singapore, 2004.
- (2) Margadonna, S.; Prassides, K. *J. Solid State Chem.* **2002**, *168*, 639.
- (3) Durand, P.; Darling, G. R.; Dubitsky, Y.; Zaopo, A.; Rosseinsky, M. *J. Nat. Mater.* **2003**, *2*, 605.
- (4) Iwasa, Y.; Takenobu, T. *J. Phys.: Condens. Matter* **2003**, *15*, R495.
- (5) Margadonna, S.; Iwasa, Y.; Takenobu, T.; Prassides, K. *Struct. Bonding* **2004**, *109*, 127.
- (6) Koch, E.; Gunnarsson, O.; Martin, R. M. *Phys. Rev. Lett.* **1999**, *83*, 620.
- (7) Capone, M.; Fabrizio, M.; Castellani, C.; Tosatti, E. *Science* **2002**, *296*, 2364.

- (8) Rosseinsky, M. J.; Murphy, D. W.; Fleming, R. M.; Zhou, O. *Nature* **1993**, *364*, 425.
- (9) Allen, K. M.; Heyes, S. J.; Rosseinsky, M. J. *J. Mater. Chem.* **1996**, *6*, 1445.
- (10) Iwasa, Y.; Shimoda, H.; Palstra, T. T.; Maniwa, Y.; Zhou, O.; Mitani, T. *Phys. Rev. B* **1996**, *53*, R8836.
- (11) Prassides, K.; Margadonna, S.; Arcon, D.; Lappas, A.; Shimoda, H.; Iwasa, Y. *J. Am. Chem. Soc.* **1999**, *121*, 11227.
- (12) Tou, H.; Maniwa, Y.; Iwasa, Y.; Shimoda, H.; Mitani, T. *Phys. Rev. B* **2000**, *62*, R775.
- (13) Simon, F.; Jánossy, A.; Murányi, F.; Fehér, T.; Shimoda, H.; Iwasa, Y.; Forró, L. *Phys. Rev. B* **2000**, *61*, R3826.
- (14) Kitano, H.; Matsuo, R.; Miwa, K.; Maeda, A.; Takenobu, T.; Iwasa, Y.; Mitani, T. *Phys. Rev. Lett.* **2002**, *88*, 096401.
- (15) Zhou, O.; Palstra, T. T. M.; Iwasa, Y.; Fleming, R. M.; Hebard, A. F.; Sulewski, P. E.; Murphy, D. W.; Zegarski, B. R. *Phys. Rev. B* **1995**, *52*, 483.
- (16) Ishii, K.; Watanuki, T.; Fujiwara, A.; Suematsu, H.; Iwasa, Y.; Shimoda, H.; Mitani, T.; Nakao, H.; Fujii, Y.; Murakami, Y.; Kawada, H. *Phys. Rev. B* **1999**, *59*, 3956.
- (17) Margadonna, S.; Prassides, K.; Shimoda, H.; Takenobu, T.; Iwasa, Y. *Phys. Rev. B* **2001**, *64*, 132414.
- (18) Margadonna, S. *New Diamond Front. Carbon Technol.* **2002**, *12*, 287.

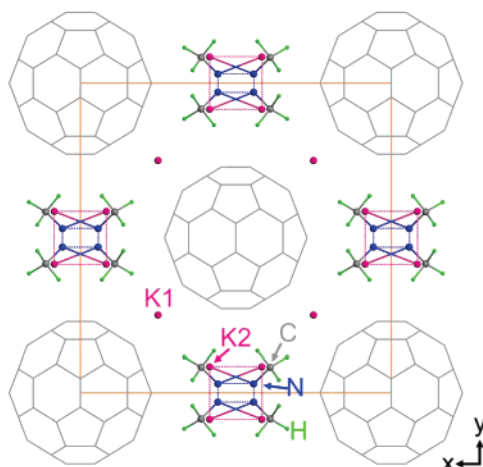


Figure 1. Basal-plane projection of the structure of methylaminated potassium fulleride ($\text{CH}_3\text{NH}_2\text{K}_3\text{C}_{60}$) at ambient temperature. The $\text{K}^+-\text{NH}_2-\text{CH}_3$ units are disordered over the corners of two interpenetrating rectangles per octahedral site, whereas K^+ the ions residing in the smaller tetrahedral interstices are not coordinated to CH_3NH_2 .

further, whereas the C_{60} units both retain a charge of -3 and remain in electronic contact by substituting Rb^+ at the K^+ sites of $(\text{NH}_3)\text{K}_3\text{C}_{60}$ and resulting in the family of fullerides, $(\text{NH}_3)\text{K}_{3-x}\text{Rb}_x\text{C}_{60}$ ($0 < x \leq 3$).¹⁹ In analogy with $(\text{NH}_3)\text{K}_3\text{C}_{60}$, these anisotropically expanded systems are also insulators and undergo an AF transition at low temperatures.^{19,20} However, T_N shows an anomalous non-monotonic dependence on the interfulleride separation and the Rb^+ concentration, x : it first increases to 76 K for $x = 2$ and then decreases to 58 K for $x = 3$.

We have recently been successful in extending the alkali fulleride phase diagram to include systems with co-intercalated neutral molecules larger than ammonia while retaining a structure related to close-packing and with significant electronic interactions between the C_{60}^{3-} anions. Co-intercalation of K_3C_{60} with methylamine afforded the hyperexpanded $(\text{CH}_3\text{NH}_2)\text{K}_3\text{C}_{60}$ phase, which adopted an orthorhombic crystal structure at ambient temperature featuring a significantly anisotropic lattice expansion (Figure 1).²¹ Unexpectedly, although $(\text{CH}_3\text{NH}_2)\text{K}_3\text{C}_{60}$ was found to also order antiferromagnetically by zero-field muon spin relaxation (ZF- μ^+ SR) measurements, the observed Néel temperature ($T_N \approx 10$ K) was significantly suppressed when compared with the ordering temperatures of the analogous ammoniated alkali fullerides, implying much weaker exchange interactions between the C_{60}^{3-} anions despite the comparable interfulleride spacings.²² Therefore, $(\text{CH}_3\text{NH}_2)\text{K}_3\text{C}_{60}$ is not simply another orthorhombic fulleride with a different unit-cell volume, and methylamine co-intercalation has produced a qualitatively new mechanism for determining its electronic properties. Understanding how electron-electron interactions are controlled near the metal-insulator

crossover region in highly expanded fullerides is of generic significance for all strongly correlated systems, and in this regard, $(\text{CH}_3\text{NH}_2)\text{K}_3\text{C}_{60}$ is a unique material combining very large interfulleride spacing with unusually low T_N and merits further attempts to explore its electronic properties in detail.

Here, we report the results of an EPR investigation of the electronic and magnetic states of $(\text{CH}_3\text{NH}_2)\text{K}_3\text{C}_{60}$ as a function of temperature. We present clear evidence of the transition to a long-range-ordered AF state below $T_N = 11$ K as observed in the temperature response of the EPR spin susceptibility and line width. A very broad resonance also emerges on the low-field side of the spectra below the ordering temperature and is tentatively assigned to an antiferromagnetic resonance (AFMR). The overall temperature response of the EPR signal is inconsistent with metallic behavior and the system can be best described as insulating with localized moments. We observe a very complex behavior of the line width, the spin susceptibility, and the *g*-factor anisotropy in the paramagnetic state that track the temperature evolution of crystallographic changes and could arise from an orbital disorder-order transition driven by the orientational ordering of the fulleride ions and/or static molecular Jahn-Teller deformations.

Experimental Section

The $(\text{CH}_3\text{NH}_2)\text{K}_3\text{C}_{60}$ sample used in the present work was prepared by reaction of single-phase K_3C_{60} powder with CH_3NH_2 vapor, as described before.²¹ Phase purity was confirmed by powder X-ray diffraction using a Stoe Stadi-P diffractometer. Synchrotron X-ray powder diffraction patterns were also recorded with the high-resolution powder diffractometer on beamline ID31 ($\lambda = 0.63782$ Å, $2\theta = 2-25^\circ$) at the European Synchrotron Radiation Facility (ESRF), Grenoble, France. For the temperature-dependent (4–294 K) X-band (9.6 GHz) cw-EPR experiments, the powder sample (3.6 mg) was sealed under helium (ca. 0.5 atm) in a 4 mm diameter silica tube (Wilmad Lab Glass). The EPR spectrometer was equipped with a Varian E-101 microwave bridge, a Varian rectangular TE_{102} resonance cavity, and an Oxford Cryogenics continuous-flow helium cryostat. The temperature stability was better than ± 0.1 K over the entire temperature range. Additional temperature-dependent low-frequency ($\nu_L = 209$ MHz, $m_{\text{sample}} = 37.5$ mg) and L-band ($\nu_L = 1.18$ GHz, $m_{\text{sample}} = 37.5$ mg) EPR experiments were also performed with home-built spectrometers.^{23,24}

Results

The X-band EPR spectrum of $(\text{CH}_3\text{NH}_2)\text{K}_3\text{C}_{60}$ at 294 K (Figure 2) has a Lorentzian line shape with a full width at half-maximum $\Delta H_{1/2} = 29.7(3)$ G and a *g*-factor $g = 2.0013(3)$. These parameters are comparable to those reported before for the ammoniated analogue $(\text{NH}_3)\text{K}_3\text{C}_{60}$ ($\Delta H_{1/2} = 28$ G, $g = 2.0011(3)$).^{9,10,19} No change in the line shape and only a small reduction in the line width of the EPR resonance is observed at the lower resonance frequencies of the present experiments ($\nu_L = 209$ MHz and $\nu_L = 1.18$ GHz), implying that the EPR line shape at room temperature is homogeneously broadened. The room-temperature spin susceptibility

- (19) Takenobu, T.; Muro, T.; Iwasa, Y.; Mitani, T. *Phys. Rev. Lett.* **2000**, 85, 381.
- (20) Arvanitidis, J.; Papagelis, K.; Takenobu, T.; Margiolaki, I.; Brigatti, K.; Prassides, K.; Iwasa, Y.; Lappas, A. *Physica B* **2003**, 326, 572.
- (21) Ganin, A. Y.; Takabayashi, Y.; Bridges, C. A.; Khimyak, Y. Z.; Margadonna, S.; Prassides, K.; Rosseinsky, M. J. *J. Am. Chem. Soc.* **2006**, 128, 14784.
- (22) Takabayashi, Y.; Ganin, A. Y.; Rosseinsky, M. J.; Prassides, K. *Chem. Commun.* **2007**, 870.

- (23) Cevc, P.; Blinc, R.; Eržen, V.; Arčon, D.; Zalar, B.; Mihailović, D.; Venturini, P. *Solid State Commun.* **1994**, 90, 543.
- (24) Cevc, P.; Walczak, T.; Swartz, H. M. *Curr. Top. Biophys.* **2002**, 26, 15.

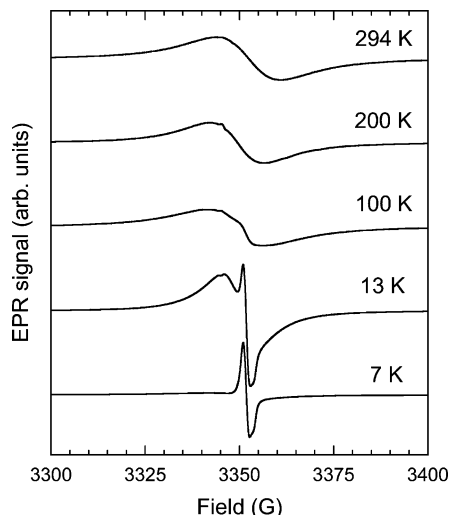


Figure 2. Temperature evolution of the X-band EPR spectra in $(CH_3NH_2)K_3C_{60}$. The narrow minority component, which appears below 120 K, is due to the presence of defects.

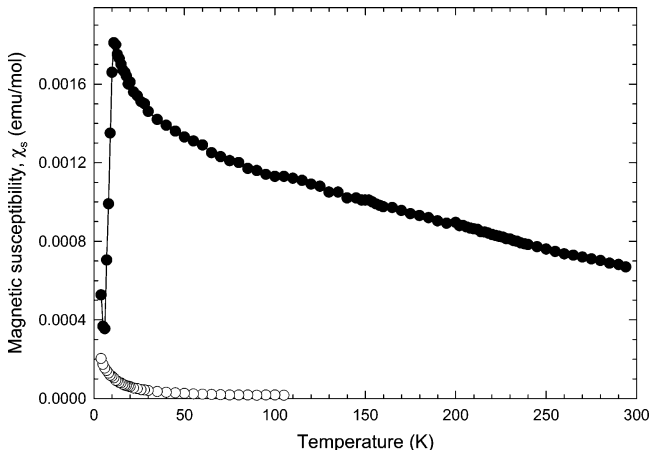


Figure 3. Temperature dependence of the X-band EPR spin susceptibility, χ_s (full circles) of $(CH_3NH_2)K_3C_{60}$. The Curie component of the susceptibility arising from the presence of defects (<1%) is also shown (open circles).

of $(CH_3NH_2)K_3C_{60}$, $\chi_s = 6.7(8) \times 10^{-4}$ emu/mol, determined from the integrated intensity of the EPR signal is somewhat smaller than that measured by SQUID magnetometry ($\chi_s = 8.8 \times 10^{-4}$ emu/mol)²¹ and is comparable to the values reported for $(NH_3)K_3C_{60}$ ($\chi_s = (5-8) \times 10^{-4}$ emu/mol)^{9,10} by the EPR technique.

The temperature evolution of the X-band EPR spectra of $(CH_3NH_2)K_3C_{60}$ at selected temperatures is shown in Figure 2. We note that, in addition to the intrinsic broad line present at all temperatures, a weak narrow ($\Delta H_{1/2} \approx 1.6$ G) resonance also becomes visible below ~ 120 K. This sharp line is attributed to paramagnetic impurities commonly present in fulleride samples, as its integrated intensity shows a Curie-law temperature response (open circles in Figure 3) with a spin-1/2 defect concentration of <1% per C_{60} molecule. The temperature dependence of the spin susceptibility, χ_s , following subtraction of the impurity line is shown in Figure 3. χ_s increases monotonically with decreasing temperature, reaching a maximum of $1.8(1) \times 10^{-3}$ emu/mol at 11 K, and then drops sharply. Such a sudden decrease in χ_s is consistent with the onset of a transition to the long-range-ordered antiferromagnetic (AF) state observed by the zero-field muon spin relaxation (ZF- μ^+ SR) technique below ~ 10 K.

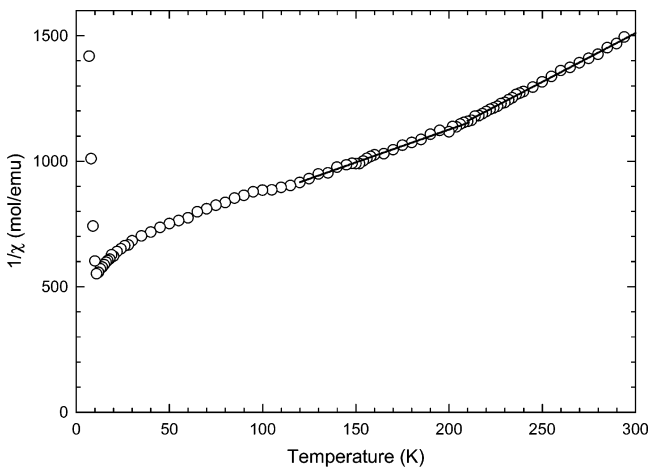


Figure 4. Temperature dependence of the reciprocal spin susceptibility, $1/\chi_s$ (full circles) of $(CH_3NH_2)K_3C_{60}$. The straight lines depict the Curie-Weiss fits of the data in the ranges 220–294 and 120–210 K.

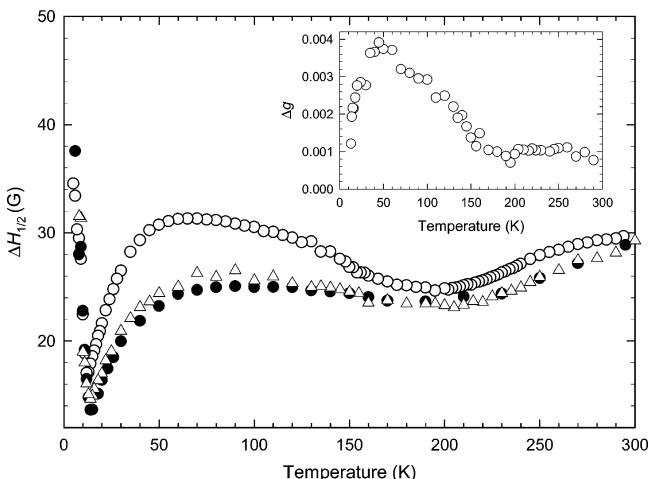


Figure 5. Temperature dependence of the EPR line width, $\Delta H_{1/2}$ of $(CH_3NH_2)K_3C_{60}$ measured in X-band (9.6 GHz, open circles), L-band (1.2 GHz, full circles), and 209 MHz (open triangles) experiments. The inset shows the temperature dependence of the g-factor anisotropy as derived from the line width data.

K^{22} The Curie-Weiss law is obeyed over the restricted temperature range of ~ 220 –294 K, yielding an effective magnetic moment, μ_{eff} , of $1.43(1) \mu_B$ per C_{60}^{3-} ion with a Weiss temperature, Θ , of $-86(2)$ K (Figure 4). A very pronounced nonlinearity is present in $\chi_s^{-1}(T)$ below 220 K. However, Curie-Weiss behavior is recovered in the temperature range ~ 120 –210 K with an increased μ_{eff} of $1.73(1) \mu_B$ per C_{60}^{3-} ion (corresponding to an $S = 1/2$ ion) and enhanced antiferromagnetic exchange interactions ($\Theta = -220(6)$ K). At lower temperatures, $\chi_s^{-1}(T)$ deviates further from the Curie-Weiss behavior, implying the presence of additional temperature-dependent AF contributions to the magnetic susceptibility, $\chi_s(T)$.

The observed changes in $\chi_s(T)$ are accompanied by a very complex behavior of the temperature dependence of the homogeneous line width, $\Delta H_{1/2}$ (Figure 5). $\Delta H_{1/2}$ measured in X-band changes considerably with the temperature decreasing between 294 and 200 K, where it reaches a minimum value of $24.6(3)$ G. Moreover, the response of $\Delta H_{1/2}$ is non-monotonic in this temperature range, as there is an inflection point at ~ 238 K, where the rate of change of $\Delta H_{1/2}$ with temperature, $d(\Delta H_{1/2})/dT$, slows down con-

siderably. This effect coincides with the observed nonlinearity in the $\chi_s^{-1}(T)$ function and the drastic change in both the effective magnetic moment of the C_{60}^{3-} units and the Weiss temperature. Below 200 K, the trend is reversed and $\Delta H_{1/2}$ starts to increase with decreasing temperature down to 65 K, where it reaches a broad maximum of 31.3(8) G. On further cooling, $\Delta H_{1/2}$ rapidly decreases toward a minimum value of 17(1) G at a temperature of 12 K, which coincides with the occurrence of the maximum in the spin susceptibility of $(CH_3NH_2)K_3C_{60}$. Below 12 K, the line width begins to increase rapidly with decreasing temperature, while at the same time, the line shape becomes progressively asymmetric and the spectral simulation with a simple Lorentzian function is no longer successful. Such line broadening provides again clear evidence of the onset of AF long-range order with a Néel temperature, $T_N = 11$ K.

Finally, we note that the difference in the line width of the EPR resonance measured at 9.6 GHz (X-band) and at low frequencies (209 MHz and 1.18 GHz) is also strongly temperature dependent. The X-band EPR line width is systematically larger than that at lower frequencies and the broadening can be ascribed to g -factor anisotropy, $\Delta g = g_{\perp} - g_{\parallel}$. Such anisotropy is nearly temperature-independent between room temperature and 200 K but progressively increases with decreasing temperature below 200 K (Figure 5 inset), approaching ~ 7 G at 50 K, corresponding to $\Delta g = g_{\perp} - g_{\parallel} \approx 4 \times 10^{-3}$. The trend reverses again below 50 K as T_N is approached from above, consistent with the development of magnetic correlations that grow rapidly on cooling.

Discussion

The EPR technique is a powerful probe of the magnetic and electronic properties of materials and has been used extensively before in the study of metallic and magnetic fulleride solids.²⁵⁻²⁸ In $(CH_3NH_2)K_3C_{60}$, there has been clear evidence from ZF- μ^+ SR measurements that static magnetic order with a broad local field distribution develops below a freezing temperature of ~ 10 K.²² The present EPR study of $(CH_3NH_2)K_3C_{60}$ is in excellent agreement with these conclusions, and the temperature evolution of both the intensity (Figure 3) and the line width (Figure 5) of the EPR resonance at low temperatures also establishes the onset of long-range AF order below $T_N = 11$ K. The EPR-derived spin susceptibility, χ_s , rapidly decreases over a few degrees below T_N , and at 4 K, the spectrum is dominated by the impurity signal. The drop in χ_s does not imply that the spin susceptibility really vanishes in the powder sample but rather that the resonance signal becomes unobservable at the lowest temperature because of the accompanying large broadening. Such behavior is entirely characteristic of the onset of AF order and is analogous to that observed in the family of ammoniated alkali fullerides, $(NH_3)K_{3-x}Rb_xC_{60}$ ($0 \leq x \leq 3$).^{9,10,13}

(25) (a) Tanigaki, K.; Prassides, K. *J. Mater. Chem.* **1995**, *5*, 1515. (b) Tanigaki, K.; Kosaka, M.; Manako, T.; Kubo, Y.; Hiroswa, I.; Uchida, K.; Holczer, K.; Prassides, K. *Chem. Phys. Lett.* **1995**, *240*, 627.
 (26) Reed, C. A.; Bolksar, R. D. *Chem. Rev.* **2000**, *100*, 1075.
 (27) Forró, L.; Mihaly, L. *Rep. Prog. Phys.* **2001**, *64*, 649.
 (28) Arcon, D.; Blinc, R. *Struct. Bonding* **2004**, *109*, 231.

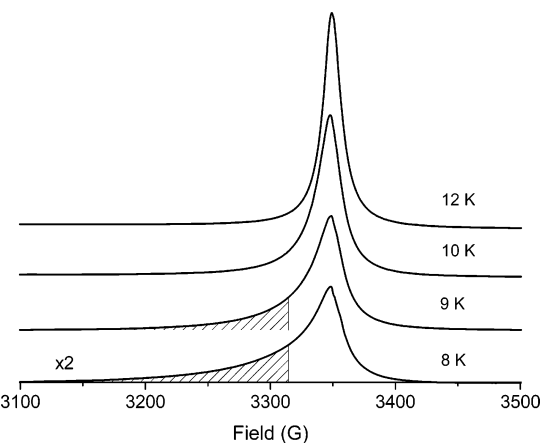


Figure 6. Integrated X-band EPR spectra of $(CH_3NH_2)K_3C_{60}$ (after subtraction of the defect line) at selected temperatures in the vicinity of T_N , showing the appearance of an additional broad resonance (shaded area) at lower fields.

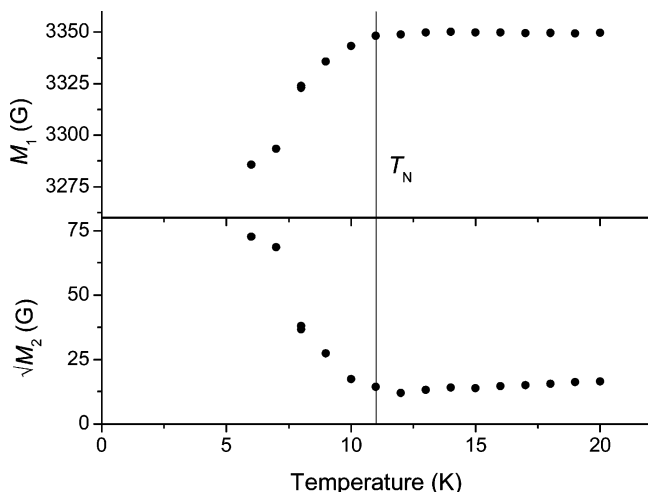


Figure 7. Temperature dependence of the first moment M_1 and the square root of the second moment $\sqrt{M_2}$ of the low-temperature X-band EPR spectra of $(CH_3NH_2)K_3C_{60}$, emphasizing the pronounced shift of M_1 to lower fields and the accompanying increase in $\sqrt{M_2}$ below $T_N = 11$ K.

To demonstrate more clearly the evolution of the measured spectra below T_N , we also show in Figure 6 the integrated X-band EPR spectra obtained after the subtraction of the impurity line. A new very broad resonance appears on the low-field side of the spectra just below T_N (shaded area in Figure 6), whereas at the same time the paramagnetic signal is rapidly suppressed. The moment analysis of the low-temperature asymmetric EPR lines comprising both signals shows that the first moment, M_1 , shifts markedly toward lower fields below T_N ; at 6 K, the center of the line has shifted by 65 G with respect to that in the paramagnetic state (Figure 7). The development of internal magnetic fields below T_N is also evident in the temperature dependence of the second moment, M_2 , which correspondingly increases drastically on cooling. This behavior of the additional EPR line at low temperature is consistent with the magnetic character of the ground state and provides preliminary evidence for its assignment as an antiferromagnetic resonance (AFMR). However, unambiguous assignment¹³ requires variable frequency measurements at fields higher than the spin-flop field, H_{SF} , for the present system.

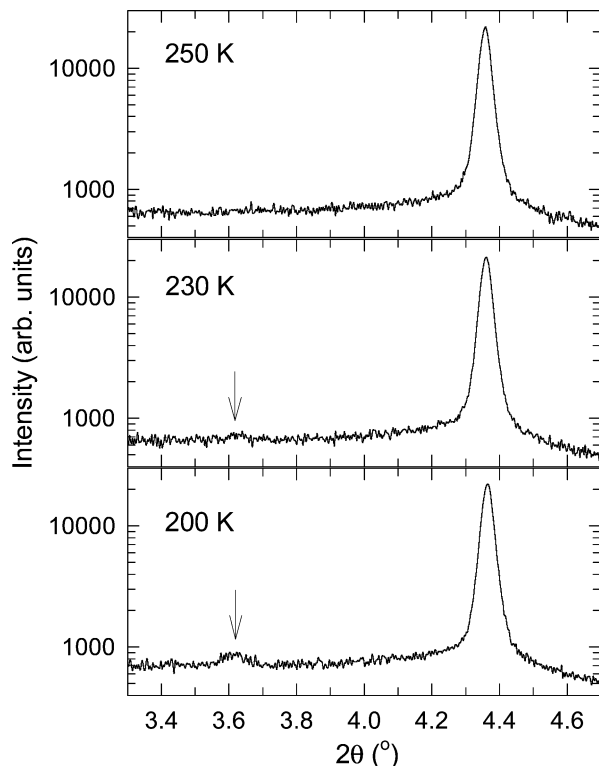


Figure 8. Selected region of the synchrotron X-ray ($\lambda = 0.63782 \text{ \AA}$) diffraction profile of $(CH_3NH_2)K_3C_{60}$ at 250, 230, and 200 K showing the appearance of the (101)/(011) forbidden Bragg reflection (indicated by an arrow) on cooling.

Several additional prominent points also arise from the present EPR results. There are subtle but well-defined anomalies in the temperature response of both χ_s and $\Delta H_{1/2}$ in the temperature range 200–250 K. Their origin can be traced to the occurrence of a structural phase transition at $T_s \approx 230 \text{ K}$, as revealed by preliminary synchrotron X-ray diffraction measurements. At high temperature, $(CH_3NH_2)K_3C_{60}$ adopts an orthorhombic structure (space group $Fmmm$) comprising orientationally disordered C_{60}^{3-} and $K^+ - NH_2 - CH_3$ units.²² However, at 230 K, a new Bragg reflection, which violates the $Fmmm$ extinction rules and indexes as (101)/(011), appears and grows in intensity continuously on cooling down to $\sim 75 \text{ K}$ (Figures 8 and 9). The structural transition is clearly manifested in the EPR data. For instance, the small g -factor anisotropy, $g_{\perp} - g_{\parallel} \approx 1 \times 10^{-3}$, at high temperature that is a consequence of the orthorhombic crystal structure starts to increase rapidly in the low-temperature phase (Figure 5 inset). This implies that the motional dynamics gradually freeze out on the EPR time scale and therefore the full g -factor anisotropy begins to recover. Moreover, the temperature evolution of the g -factor anisotropy bears a striking similarity to that of the order parameter ((101)/(011) intensity) of the structural transition (Figure 9). The sensitivity of the magnetic response, as detected by EPR, to the structural transformation implies a significant change in the electronic structure of $(CH_3NH_2)K_3C_{60}$ upon the lowering of the crystal symmetry that is tracked sensitively by the g -factor. Detailed conclusions should await determination of the low-temperature crystal structure, but we note that (i) the transition temperature, T_s , for $(CH_3NH_2)K_3C_{60}$ is much higher than those ($\sim 150 \text{ K}$) encountered in the

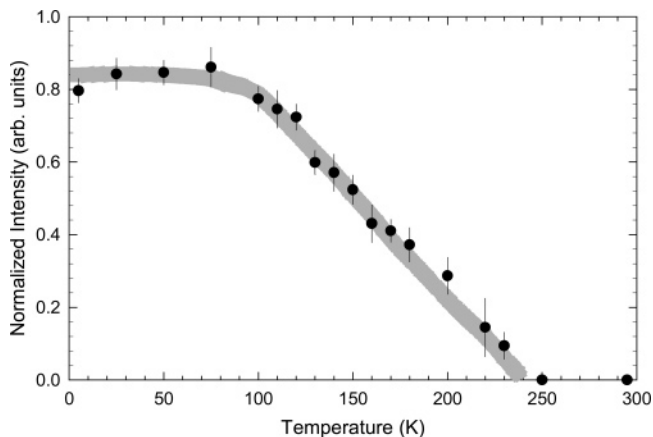


Figure 9. Temperature dependence of the normalized intensity of the (101)/(011) Bragg reflection, which is forbidden in the orthorhombic $Fmmm$ space group. The shaded gray line is a guide to the eye.

ammoniated analogues $(NH_3)K_{3-x}Rb_xC_{60}$ ($0 \leq x \leq 3$)^{16,17,19} and (ii) the symmetry-forbidden reflection in $(CH_3NH_2)K_3C_{60}$ differs from that ((110)) observed in the low-temperature phases of the ammoniated systems.^{16,17,29} Therefore, the implication is that the low-temperature orientational ordering motifs of the C_{60}^{3-} and/or the $K^+ - NH_2 - CH_3$ units in $(CH_3NH_2)K_3C_{60}$ are quite distinct from those established in the ammoniated analogues (antiferroelectric ordering of the $K^+ - NH_3$ dipoles and antiferrorotative ordering of the C_{60}^{3-} ions).

Another important question to address is also the nature of the electronic state of the $(CH_3NH_2)K_3C_{60}$ system above T_N . We note that the $\chi_s(T)$ behavior in the paramagnetic regime is atypical of both insulating localized moment and metallic systems. Although it differs drastically from what is observed for metallic fullerenes such as K_3C_{60} , the extracted values of Θ are much larger than the temperature at which the onset of 3D AF long-range order occurs ($\sim 11 \text{ K}$). A similar situation had been encountered in the ammoniated analogues $(NH_3)K_{3-x}Rb_xC_{60}$ ($0 \leq x \leq 3$) in which the EPR results above T_N were interpreted in terms of a strongly correlated metallic picture.^{9,10,13} This model was proven inappropriate by subsequent ac conductivity measurements,¹⁴ which provided unambiguous evidence for the insulating nature of the ground state in these materials. Therefore, although a definitive answer about the electronic properties of $(CH_3NH_2)K_3C_{60}$ cannot be provided by the EPR results alone, by analogy, the present material displays a phenomenology close to that expected for an insulator with localized moments.

This picture is further supported by the behavior of $\Delta H_{1/2}(T)$, which is again atypical of metallic A_3C_{60} fullerenes. In the metallic systems, the spin–lattice relaxation time, $T_1 = 2\eta/g\mu_B\Delta H_{1/2}$, is controlled by the spin–orbit coupling of the conduction electrons to the lattice and can be successfully explained by the Elliot mechanism of conduction electron EPR,³⁰ in which $T_1 = \alpha/(\delta g)^2\tau_s$, where α is a constant on the order of 1 for isotropic systems, δg is the shift of the g -factor from the free electron value, $g_e = 2.0023$, and τ_s is the relaxation time of the electrical conductivity. Therefore,

(29) Margadonna, S.; Prassides, K.; Shimoda, H.; Iwasa, Y.; Mezouar, M. *Europhys. Lett.* **2001**, *56*, 61.

(30) Elliot, R. J. *Phys. Rev.* **1954**, *96*, 266.

the line width is expected to decrease gradually with decreasing temperature, in sharp contrast to what is observed in $(\text{CH}_3\text{NH}_2)\text{K}_3\text{C}_{60}$. In addition, the development of a sizable *g*-factor anisotropy on cooling below 200 K ($g_{\perp} - g_{\parallel} \approx 4 \times 10^{-3}$ at 50 K, Figure 5 inset) is again inconsistent with a metallic ground state for $(\text{CH}_3\text{NH}_2)\text{K}_3\text{C}_{60}$, because for a metal the *g*-factor anisotropy is expected to average out through the diffusion of the conduction electrons.

Moreover, the temperature dependence of $\Delta H_{1/2}$ in the paramagnetic state (Figure 5) is very intriguing and considerably more complex than that observed previously for the ammoniated analogues.^{9,10,19} In the latter, $\Delta H_{1/2}$ increases monotonically (but significantly more weakly than in $(\text{CH}_3\text{NH}_2)\text{K}_3\text{C}_{60}$) on cooling between room temperature and the onset of the structural phase transition at ~ 150 K. This has been attributed to the gradual slowing down of the reorientational motion of the fulleride ions,³¹ as fluctuations at the Larmor frequency will lead to the broadening of the EPR line. Below the structural transition, line narrowing is observed, following the freezing out of the C_{60}^{3-} rotations and the increase in molecular order. In $(\text{CH}_3\text{NH}_2)\text{K}_3\text{C}_{60}$, the line width first decreases on cooling below 294 K, exhibiting a change in slope only at the structural transition near 230 K. The trend is reversed below 200 K and is accompanied by large increases in both the effective magnetic moment per C_{60}^{3-} unit and the Weiss temperature. One possible explanation of these responses is that they are associated with an orbital disorder–order transition in this temperature range. The reduced spin moment at high *T* could originate from the presence of an orbital contribution, which is removed on cooling by some electronic and/or structural distortion removing the orbital degeneracy. The unusually large Weiss temperatures ($\Theta \gg T_N$) may then also arise from the presence of an orbital moment, which gives rise to low-lying states that cannot be accounted for by a simple Curie–Weiss behavior. Two mechanisms can be then envisaged as the driving force of orbital ordering below ~ 200 K. First, it has been established that in the analogous fulleride $(\text{NH}_3)\text{K}_3\text{C}_{60}$, there is strong coupling among the orbital, lattice (orientational), and magnetic degrees of freedom and that the structural phase transition leads to antiferrorotational ordering of the C_{60}^{3-} units,¹⁷ which gives rise to distinct t_{1u} orbital ordering that modulates the intermolecular exchange interactions. A similar scenario implicating a t_{1u} orbital disorder–order transition driven by the orientational ordering motif of the C_{60}^{3-} units at temperatures below the structural phase change could account for the observed anomalies in the temperature response of χ_s , $\Delta H_{1/2}$, and Δg . Alternatively, the effects can be of purely electronic origin involving Jahn–Teller (JT) deformations of the highly symmetric C_{60}^{3-} anions such as those directly observed in the fulleride salt $[\text{PPN}]_3\text{C}_{60}$ (PPN^+ = bis(triphenylphosphine)iminium ion).³² A crossover from a high-temperature dynamic JT to a low-temperature static JT distortion of the fulleride ions will be also entirely consistent with the

observed temperature dependence of $\Delta H_{1/2}$ and the change in μ_{eff} and Θ on cooling. Very importantly, it will also have a direct impact on the value of the electronic *g*-factor anisotropy, Δg , which in the static JT regime is proportional to (λ/Δ) , where λ is the spin–orbit coupling constant and Δ is the JT splitting.³³ The structural distortion in the paramagnetic state can be associated with the removal of the t_{1u} orbital degeneracy. At high temperature, this effect has a weak influence on the electronic structure of $(\text{CH}_3\text{NH}_2)\text{K}_3\text{C}_{60}$ and gives rise to a small value of the *g*-factor anisotropy. The lifting of the orbital degeneracy is clearly enhanced at the structural transition and affects the magnitude of Δg . As the distortion increases continuously on cooling, there is a concomitant increase in the orbital degeneracy lifting, which further changes Δg and is sensitively tracked by it. We note that the magnitude of the measured *g*-factor anisotropy and the temperature range in which it becomes important in $(\text{CH}_3\text{NH}_2)\text{K}_3\text{C}_{60}$ are comparable to those observed by EPR in $(\text{P}(\text{C}_6\text{H}_5)_4)_2\text{C}_{60}\text{I}$, for which a dynamic-to-static JT transition was also implicated to account for the electronic properties.³⁴

Conclusions

In conclusion, the hyperexpanded $(\text{CH}_3\text{NH}_2)\text{K}_3\text{C}_{60}$ fulleride retains electronic contact between the C_{60}^{3-} anions and shows a transition to a long-range AF state at a temperature ($T_N = 11$ K) substantially lower than those ($T_N \approx 70$ –80 K) observed in the ammoniated $(\text{NH}_3)_{3-x}\text{Rb}_x\text{C}_{60}$ ($0 \leq x \leq 3$) analogues at comparable interfulleride spacings. This suggests that the exchange interactions between the fulleride anions in the methylaminated phase at low temperature differ markedly from those in the ammonia-based materials. This is consistent with the strong differences observed in the temperature dependence of the EPR line width reported here from those of the $(\text{NH}_3)\text{A}_3\text{C}_{60}$ phases. The variation of the EPR resonance in the paramagnetic regime is more consistent with the assignment of the $(\text{CH}_3\text{NH}_2)\text{K}_3\text{C}_{60}$ electronic state as that of an insulator with localized moments rather than as that of a metallic system. However, both the EPR-derived spin susceptibility and EPR line width show unusually complicated dependence on temperature, necessitating a more complex description of the electronic properties of this fulleride with the magnetic exchange interactions responding sensitively to the occurrence of a structural phase transition. It appears likely that the structural changes on cooling, which are mirrored by the evolution of the *g*-factor anisotropy measured by EPR, are accompanied by an orbital disorder–order transition driven by the strong coupling between the orientational, electronic, and magnetic degrees of freedom and/or the onset of static JT distortions at the molecular level that modulate the lifting of the t_{1u} orbital degeneracy.

Acknowledgment. We thank the EPSRC for financial support (M.J.R., K.P.), the ESRF for provision of beamtime, and Dr. A. N. Fitch (ESRF) for help with the diffraction experiments.

CM070016P

(31) Margadonna, S.; Prassides, K.; Neumann, D. A.; Shimoda, H.; Iwasa, Y. *Phys. Rev. B* **1999**, *59*, 243.
 (32) Bhryappa, P.; Paul, P.; Stinchcombe, J.; Boyd, P. D. W.; Reed, C. A. *J. Am. Chem. Soc.* **1993**, *115*, 11004.

(33) Chancey, C. C.; O'Brien, M. C. M. *The Jahn-Teller Effect in C₆₀ and Other Icosahedral Complexes*; Princeton University Press: Princeton, NJ, 1997.
 (34) Gotschy, B.; Keil, M.; Klos, H.; Rystau, I. *Solid State Commun.* **1994**, *92*, 935.